INSTITUTE OF PHYSICS PUBLISHING NANOTECHNOLOGY
Nanotechnology **17** (2006) 3832–3837 doi:10.1088/0957-4484/17/15/038

A dynamic Monte Carlo study of the *in situ* growth of a substance deposited using electron-beam-induced deposition

Zhi-Quan Liu[1], **Kazutaka Mitsuishi and Kazuo Furuya**

High Voltage Electron Microscopy Station, National Institute for Materials Science (NIMS), 3-13 Sakura, Tsukuba 305-0003, Japan

E-mail: zhiquanliu@yahoo.com and liu.zhiquan@nims.go.jp

Received 7 May 2006, in final form 20 June 2006
Published 6 July 2006
Online at stacks.iop.org/Nano/17/3832

Abstract
The *in situ* growth of a deposit in electron-beam-induced deposition (EBID) was studied by dynamic Monte Carlo simulation, showing first the preferential growth of deposit along the incident direction of the electron beam. The effects of electron energy, probe size, substrate thickness, and deposit (or substrate) composition on EBID were investigated and discussed, considering the electron scattering of not only secondary electrons but also primary and backscattered electrons in solids. By including the depositions at not only the top but also the bottom surfaces of the substrate, the growth model of the deposit in EBID was modified. Concerning the resolution of EBID, a small lateral size can be achieved on the deposit (or substrate) containing light atoms using a high-energy electron beam with a fine probe size.

(Some figures in this article are in colour only in the electronic version)

1. Introduction

In recent years, growing interest has been paid to the usage of electron beams in nanotechnology due to their flexibility and accuracy [1]. Among different technologies using fine electron beams, electron-beam lithography (EBL) [2] and electron-beam-induced deposition (EBID) [3] are two important ones in the area of nanofabrication. Since EBL is performed on a mask or resist and needs further processing like lifting and etching, it is not suitable for three-dimensional fabrication. EBID can add desired materials on any position of substrate directly. Thus it was considered to be a potential method to substitute for the traditional method of microelectronic fabrication involving resist lithography, plasmochemical treatment, and lift-off processes.

The process of EBID includes electron–solid interactions among three entities, which are the electron beam, the substrate, and the gas precursor [4]. These interactions are so complicated that, so far, parts of them are still unknown and need to be investigated further. Although many experiments have been carried out to study the mechanism of EBID, the results obtained mainly depend on the individual experimental conditions [5, 6]. The Monte Carlo simulation method is a powerful theoretical tool for the evaluation of the electron–solid interactions [7], which can specify different experimental conditions and has been widely used in electron probe microanalysis, electron spectroscopy, and electron microscopy [8, 9]. However, this method has seldom been used in EBID, and was just used to estimate the ultimate resolution of a dot [10], which only corresponds to the very initial stage (i.e. the nucleation stage) of EBID. In order to fulfill the purpose of controlled fabrication with a desired size, shape, and position [11], an understanding of the full EBID process, including both nucleation and growth, is more important, considering its real application in three-dimensional nanofabrication with not only dots but also tips and wires.

In the present study, the *in situ* growth of a deposit was systematically investigated by Monte Carlo simulation, considering the effects of the electron beam and the substrate (deposit) on EBID. The preferential growth of a bottom deposit along the incident direction of the electron beam was first revealed, and the role of forward-scattered electrons

[1] Author to whom any correspondence should be addressed.

was discussed. These results are essential and important for understanding not only EBID but also other electron–solid interaction processes such as EBL, especially when a substrate of nanometre size is used in these processes.

2. Methods

A dynamic Monte Carlo profile simulator including the secondary electrons generated in the already-grown deposit, as suggested first by Silvis-Cividjian *et al* [12], was designed to simulate the process of EBID as described elsewhere [13]. The single scattering model using the Rutherford cross section was employed to perform the Monte Carlo calculations, and the fast secondary-electron model was selected to simulate the generation of secondary electrons, as proposed by Joy [14]. After a primary electron (PE) is injected into a solid, the trajectories of all electron species, including PE and the generated backscattered electrons (BSE) and secondary electrons (SE), are tracked; it is essential to include the contributions of not only SE but also PE and BSE. The growth of the deposit is considered to be an aggregation of $0.3 \times 0.3 \times 0.3$ nm^3 cubes in three dimensions. When a scattered electron escapes from the solid, depending on the electron energy, the probability of the occurrence of a deposit (cube) is decided by the dissociation cross section of the precursor gas.

Because experiments to measure dissociation cross section are difficult to perform, complete data is only available for simple gases such as H_2, N_2 and CO. For most of the gas precursors used in EBID, there are not enough experimental values, so many authors have used modified models. As we know, carbon tetrafluoride (CF_4) is widely used in plasma-assisted material processing, and has a variety of databases concerning electron interactions [15]. The dissociation cross sections of CF_4 and other fluoroalkanes have a threshold at 10–50 eV and slowly decay, with a peak at around 100 keV [16]. Therefore, a plot of dissociation cross section with a peak at around 100 eV and a threshold at 35.5 eV was adopted in this work (the mean free path of a 35.5 eV electron is about 0.1 Å). Within the first Born approximation, the plot has a shape of $\sigma = (A/E)\ln(E/B)$, where E is the incident electron energy and A and B are constants [16].

During simulation, a PE injects into the substrate normal to its top surface, which corresponds to the spot mode without movement of the electron beam. For simplicity, simulations were carried out to deposit a material onto the same substrate, and the already-grown deposit acts as a substrate in the following deposition. Changes of electron energy (20, 100 and 200 keV), probe size (0, 1 and 2 nm), substrate thickness ($0.3 \times 0.3 \times 0.3$ nm^3 cube; 1, 5, 10, 50 and 100 nm-thick films), and deposit composition (carbon and tungsten) were included in the simulation to investigate their effects.

3. Results

3.1. Variation of electron energy

Figure 1 shows the simulated deposition of a tungsten tip on a tungsten point substrate ($0.3 \times 0.3 \times 0.3$ nm^3 cube) using a 0 nm electron probe with different energies. The cross-sectional profiles of tips simulated with 600 000 PEs

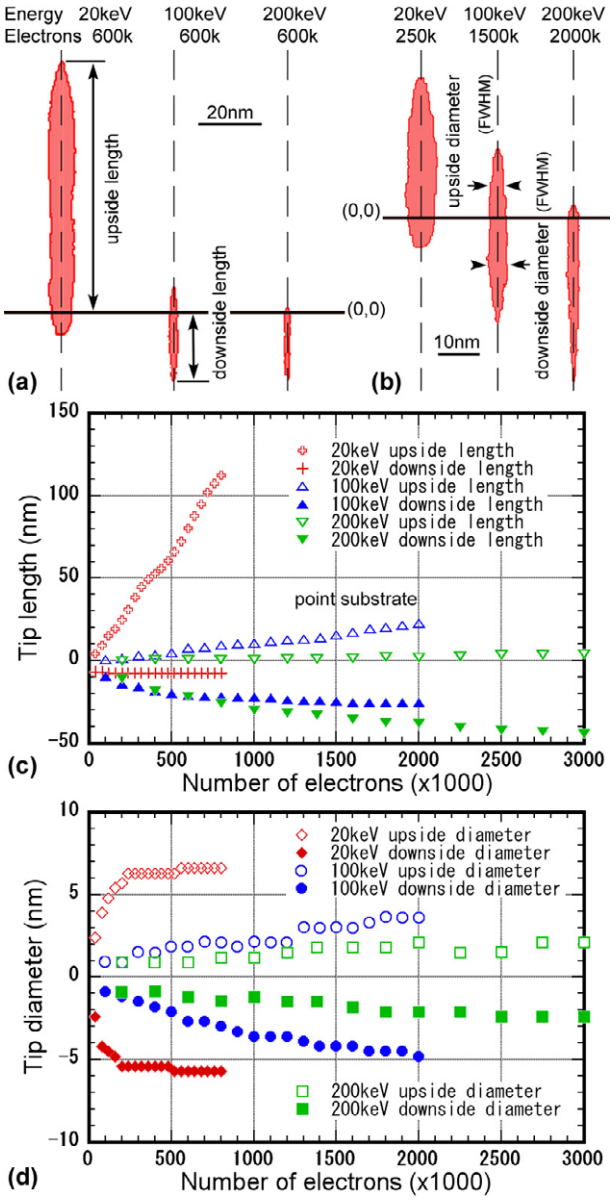

Figure 1. Growth of a tungsten tip on a tungsten point substrate using 20, 100 and 200 keV primary electrons (PE) with a 0 nm probe size. (a) Tip profiles simulated with 600 000 PEs. (b) Tip profiles with a similar length of 40 nm. (c) Plots of tip length. (d) Plots of tip FWHM diameter.

are shown in figure 1(a). Each tip consists of an upside part and a downside part, and the tips simulated with 100 and 200 keV electrons have a longer downside parts. To deposit a tip with a total length of about 40 nm, 250 thousand 20 keV electrons are needed, while the number of 100 and 200 keV electrons is six times and eight times larger, as shown in figure 1(b). The tip lengths and FWHM (full width at half maximum) diameters simulated with different electron energies are plotted in figures 1(c) and (d), respectively. The horizontal coordinate is the number of incident electrons. For comparison, negative values are assigned to the length and diameter (vertical coordinate) of the downside part of tips. As shown in figure 1(c), all upside parts grow linearly while downside parts turn to saturation for different electron energies.

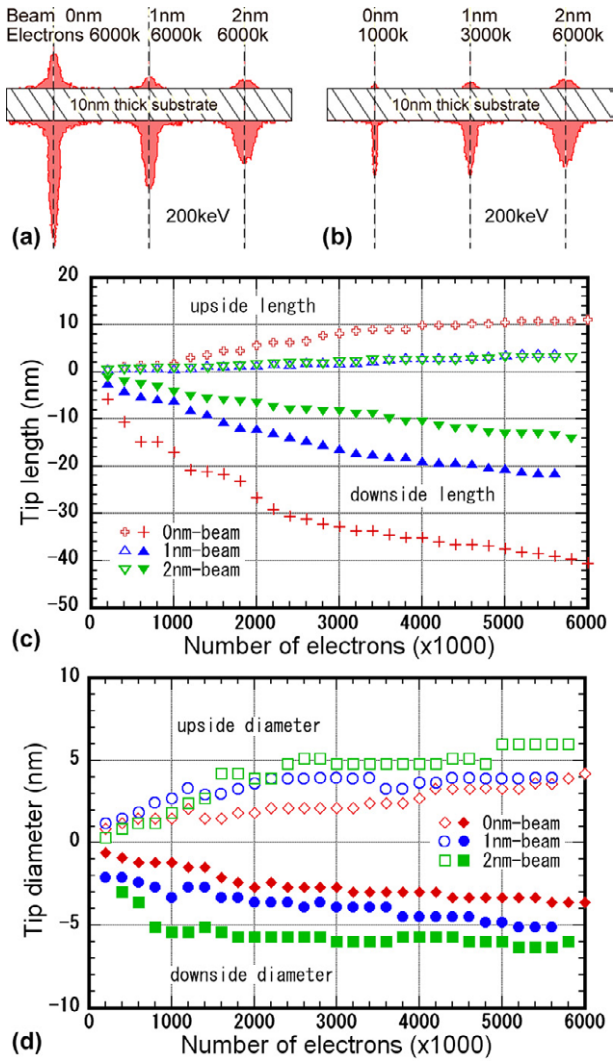

Figure 2. Deposition of a tungsten tip on a 10 nm-thick tungsten film using 200 keV primary electrons (PEs) with probe sizes of 0, 1 and 2 nm. (a) Tip profiles simulated with 6 million PEs. (b) Tip profiles with a similar length of 19 nm. (c) Plots of tip length. (d) Plots of tip FWHM diameter.

However, the saturated length of the downside part and the growth rate of the upside part vary with electron energy. Considering the lateral size of the tip in figure 1(d), the tip diameter also varies with the energy of the primary electrons and turns to saturation ultimately. It is clear that the growth rate of high-energy electrons is low. For example, the linear growth rate of the upside part in figure 1(c) decreases from 141.14 nm per thousand electrons for 20 keV electrons, 11.19 nm per thousand electrons for 100 keV electrons, to 1.42 nm per thousand electrons for 200 keV electrons. An advantage of using high-energy electrons is achieving smaller lateral size, as shown in figure 1(d), so as to improve the aspect ratio of the deposit. The tip aspect ratio calculated with the whole tip length and the projected diameter increases from 6.38 to 11.17 and 19.14 by increasing the electron energy from 20 keV to 100 keV and 200 keV in figure 1(b).

3.2. Variation of probe size

Figure 2 presents the effects of probe size on the deposition of a tungsten tip on a 10 nm-thick tungsten film. Figure 2(a) shows the tips simulated with 6 million 200 keV electrons with probe sizes of 0, 1 and 2 nm, while figure 2(b) shows tips with similar lengths (19 nm) using different probe sizes. The plots of tip lengths and FWHM diameters are shown in figures 2(c) and (d), respectively. Again, deposition happened on both the top and bottom surfaces of a 10 nm-thick film substrate to deposit both top tips and longer bottom tips. The growth rate of the deposit decreases with an increase in probe size. For example, the upside growth rate in figure 2(c) is 1.75 nm per thousand electrons for a 0 nm probe, 0.63 nm per thousand electrons for a 1 nm probe, and 0.48 nm per thousand electrons for a 2 nm probe, respectively. With the same number of incident electrons, the length of the bottom tip also decreases with an increase in probe size, as shown in figure 2(c). However, the probe size will not affect the final saturated downside length, which only depends on the electron energy (or beam penetration depth) and substrate thickness. Undoubtedly, the lateral size is increased by using a larger probe size, and the aspect ratio of the tip is decreased, as shown in figure 2(b).

3.3. Variation of substrate thickness

The profiles of tips deposited on 10, 50 and 100 nm-thick films using 20 and 200 keV primary electrons are shown in figures 3(a) and (b), respectively. A bottom tip was absent on the 50 nm-thick substrate using 20 keV electrons in figure 3(a), but was deposited using 200 keV electrons in figure 3(b). The plots of the tip length on 0.3 nm cube, 10, 50 and 100 nm-thick substrates are shown in figure 3(c) for 20 keV electrons, and in figure 3(d) for 200 keV electrons. The substrate thickness has less effect on the deposition of the upside parts, which have similar growth rates and lateral sizes. The upside growth rate using 20 keV electrons in figure 3(c) is in the range 113.95–141.14 nm per thousand electrons, while that using 200 keV electrons in figure 3(d) ranges from 1.42 to 1.77 nm per thousand electrons. However, the deposition of the bottom tip strongly depends on the substrate thickness, especially for high-energy electrons, as shown in figures 3(b) and (d). The thinner the substrate is, the longer the saturated downside parts will be. If we only consider the downside part of the tip, a higher aspect ratio can be obtained on a thinner substrate.

3.4. Comparison of carbon and tungsten deposition

Since contamination writing with carbon has the longest history and tungsten gases (WF_6, $W(CO)_6$) are most widely used in EBID, the deposition of these two materials was investigated. The comparison of carbon-on-carbon and tungsten-on-tungsten deposition on 1, 5 and 10 nm-thick films is shown in figure 4. Figure 4(a) shows the simulated profiles of tips using 400 thousand 20 keV primary electrons. A rigid comparison of their growth rates is meaningless, because a uniform dissociation cross section was adopted for both carbon and tungsten in the simulation, which should be different for various gas molecules in real experiments. However, figure 4(a) qualitatively tells us that the growth of a downside

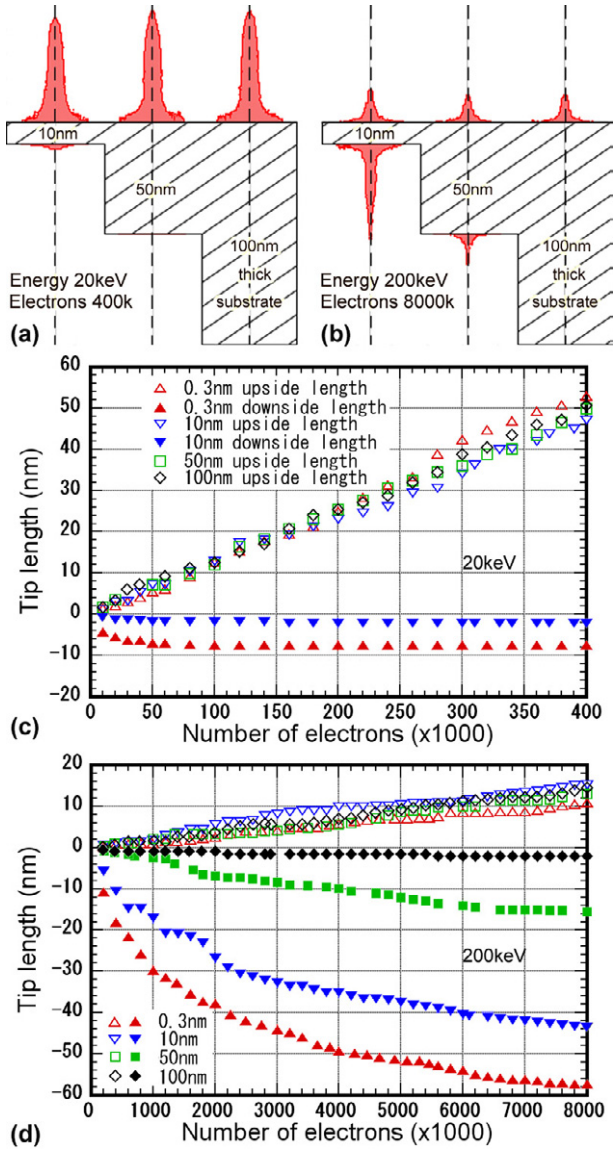

Figure 3. Effects of substrate thickness on the deposition of a tungsten tip using 20 and 200 keV primary electrons with 0 nm probe size. (a) Tip profiles simulated with 400 thousand 20 keV PEs. (b) Tip profiles simulated with 8 million 200 keV PEs. (c) Plots of tip length using 20 keV PEs. (d) Plots of tip length using 200 keV PEs.

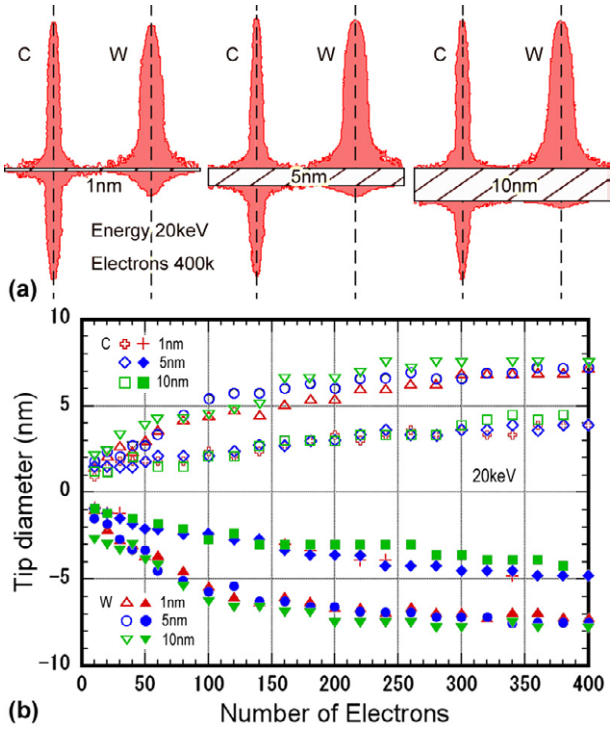

Figure 4. Comparison of the deposition of carbon and tungsten tips on their own substrates. (a) Profiles of carbon tips on a carbon substrate and tungsten tips on a tungsten substrate, simulated with 400 thousand 20 keV PEs on 1, 5 and 10 nm-thick films. (b) Plots of FWHM diameters of carbon and tungsten tips on their substrates.

tip is easier for carbon than for tungsten. Considering their lateral sizes, as shown in figure 4(b), the diameter of a carbon tip is always smaller than that of a tungsten tip. Thus, the carbon tip has a higher aspect ratio and is sharper than the tungsten tip, as shown in figure 4(a).

4. Discussion

4.1. Electron–solid interactions affecting the EBID resolution and the bottom deposition

In order to understand the different aspects of electron-beam-induced deposition, the electron–solid interactions involved in this process have to be considered. As we know, low-energy secondary electrons play an important role in EBID [17]. However, the yield of secondary electrons decreases as the energy of incident electrons increases, which results in a decreasing growth rate. Moreover, by increasing the energy of incident electrons, the lateral spread of secondary electrons will decrease and the interaction area between electrons and solids moves forward along the incident direction. As a result, the lateral size of the deposit decreases and a longer downside part was deposited using a higher electron energy, as shown in figure 1. As the incident electrons distribute within the size of electron probe that has a Gaussian shape, an increase in probe size will increase the incident area of primary electrons and decrease its incident density (the number of PEs per unit area). Hence the lateral size increases and the vertical growth rate of deposit decreases, as shown in figure 2. The substrate thickness has less effect on the growth of the upside part, as shown in figure 3. However, the growth of the downside part depends on the substrate thickness, the threshold of which is determined by the penetration depth of the electron beam. A downside part will be deposited if the substrate thickness is below the penetration depth of the electron beam. Considering electron scattering in carbon and tungsten, carbon has a smaller scattering angle and a longer mean free path than tungsten, resulting in a smaller lateral energy spread and a larger penetration depth. Therefore, the carbon tip has a smaller lateral size and a longer downside part, as shown in figure 4.

So far, all investigations were mainly focused on deposition on the top surface of the substrate [18, 19]. Deposition on the bottom surface of the substrate has not been observed experimentally before, which should be due

to the usage of bulk substrates and low-energy electrons in previous studies. Although a 10 nm-thick substrate and 200 keV electrons were used in a theoretical simulation, it still shows the dominant growth of the top tip, which has a comparable growth rate with the bottom tip at the initial stage [12]. However, according to our investigation, the bottom tip has a higher growth rate than the top tip at the beginning stage. As we know, the deposition of an upside part (top tip) depends on the backward-scattered electrons, including BSEs and SEs, emerging from the top surface of substrate, while the deposition of a downside part (bottom tip) relies on the forward-scattered electrons, including PEs and SEs, that escaping from the bottom surface. Although, for an individual SE, it can be scattered in all directions, the emission site of an SE is determined by the trajectories of the PE or BSE. In fact, only a few high-energy SEs have sufficient energy to travel a long distance in the specimen. Most low-energy SEs do not travel, thus their locations mark out the trajectories of the PEs and BSEs. That is to say, the distribution of SEs is convoluted by the trajectories of PEs and BSEs. As a PE is mainly forward-scattered after entering a solid, the distribution of SEs also elongates along the incident direction of the electron beam, which results in the deposition of a bottom tip. Within the beam penetration depth, the number of forward-scattered electrons is larger than that of backward-scattered electrons, which results in a higher growth rate of the bottom tip. As both the already-grown top and bottom tips act as new substrates for further deposition, the total thickness of substrate (including the original substrate and the top and bottom tips) will increase to exceed the penetration depth of electron beam. At this stage, no electrons can escape from the bottom surface anymore and the bottom tip turns to saturation.

4.2. In situ top–bottom growth model and the role of primary electrons

Thus the *in situ* growth model of the deposit, including both top and bottom tips, can be summarized as follows: at the initial stage, a bottom tip is preferentially deposited with a higher growth rate and then turns to saturation, while the top tip keeps growing linearly with a low but constant growth rate; the growth of the top tip becomes dominant after the saturation of the bottom tip. This modified growth model includes the contributions of not only secondary electrons and back-scattered electrons, but also primary electrons. It has been reported recently that primary electrons are the dominant species responsible for the vertical growth of deposit at the top surface of the substrate [20]. Our work demonstrates their role on deposition at the bottom surface of the substrate. In principle, primary electrons contribute to the bottom deposition in two ways: generating and restricting the distribution of secondary electrons along the beam axis, and participating in the deposition directly by themselves. In the fast secondary-electron (FSE) model, the yield of FSEs (typically from 0.001 to 0.1) is quite small compared with normal SE yields (usually between 0.1 and 1) [14]. As different electrons were defined by their energy, and the threshold of dissociation cross section was chosen at 35.5 eV, the contribution of primary electrons has been highlighted here. The aim of this work is to modify the growth model of the deposit containing both top and bottom parts, and to investigate the effects of electron energy, probe size, substrate thickness and composition on the EBID process. Although high SE yield and a low threshold of dissociation cross section can increase the contribution of secondary electrons and hence quantitatively increase the growth rate of deposit, their influences on our results qualitatively count for little. Moreover, the above theoretical results have been verified by our recent experimental depositions using 200 and 400 keV electrons, which will be summarized later.

It should be noted that, although the effects of electron energy, probe size, substrate thickness, and deposit (substrate) composition on the growth rate and resolution of EBID were investigated here, other factors such as substrate temperature and gas pressure were not studied, since they were not included in the dynamic Monte Carlo profile simulator. As we know, the possibility (P) of atom deposition on a surface is a multiplication of the dissociation cross section (σ) with the density (or coverage, N) of precursor molecules adsorbed on the surface. As an estimated σ was adopted in the simulation, its multiplication by even an accurate N is still uncertain. For simplicity, the possibility of deposition was only determined by σ regardless of N in this simulation (i.e. the coverage of molecule was assumed to be 100%). Thus the parameters of substrate temperature and gas pressure, which determine the density of adsorbed precursor molecules at the substrate surface, were not considered in the design of the simulator. In fact, among electron, substrate, and gas precursor in EBID, this work mainly focuses on the interactions between electron/substrate and electron/precursor but not substrate/precursor, to study the top-bottom growth behaviour of the deposit. Although substrate temperature and gas pressure (or inhomogeneity) can significantly influence the growth rate of a deposit [21], they have less impact on the profile (or shape) of the deposit, and their effects can be subtracted during the comparison of the top and bottom deposits. Therefore, the exclusion of substrate temperature and gas pressure does not ruin the qualitative results presented in this manuscript. However, for the practical application of this program to predict and quantify the experimental procedure, these parameters should be included in the simulator, based on the achievement of other accurate data such as dissociation cross section.

4.3. Outlook

Attention should be paid to the preferential growth of the bottom deposit in the application of EBID, since the devices (or substrates) used for fabrication are becoming smaller and smaller now. On the other hand, due to its higher growth rate at the initial stage, one can also intend to deposit structures only on the bottom surface of the substrate within a very short time. To avoid or to use the deposition of the bottom deposit, a gas control system is necessary to supply precursor molecules only on the top or bottom surfaces of the substrate.

5. Conclusions

In conclusion, the effects of electron energy, probe size, substrate thickness, and deposit (substrate) composition on EBID were studied by dynamic Monte Carlo simulation. The preferential bottom growth of the deposit was revealed, which

is counter-intuitive and was missed in the old models. The new top–bottom growth model was discussed, considering the electron scattering of primary, backscattered, and secondary electrons with solids. Backward-scattered electrons contribute to the growth of top deposit facing the incident beam, while forward-scattered electrons contribute to deposition at the bottom surface of the substrate. Primary electrons also play an important role in the EBID process. An increase in electron energy improves the resolution of EBID but also reduces its productivity. By decreasing the probe size, both resolution and productivity can be improved. The substrate thickness has less effect on the resolution of EBID, but it influences the saturated length of the bottom tip. Comparing the deposition of carbon and tungsten, better resolution can be obtained for materials of low atomic number.

References

[1] Storm A J, Chen J H, Ling X S, Zandbergen H W and Dekker C 2003 Fabrication of solid-state nanopores with single-nanometre precision *Nat. Mater.* **2** 537

[2] Liu K, Avouris Ph, Bucchignano J, Martel R, Sun S and Michl J 2002 Simple fabrication scheme for sub-10 nm electrode gaps using electron beam lithography *Appl. Phys. Lett.* **80** 865

[3] Boero G, Utke I, Bret T, Quack N, Todorova M, Mouaziz S, Kejik P, Brugger J, Popovic R S and Hoffmann P 2004 Submicrometer hall devices fabricated by focused electron-beam-induced deposition *Appl. Phys. Lett.* **86** 042503

[4] Koops H W P, Kaya A and Weber M 1995 Fabrication and characterization of platinum nanocrystalline material grown by electron-beam induced deposition *J. Vac. Sci. Technol.* B **13** 2400

[5] Beaulieu D, Ding Y, Wang Z L and Lackey W J 2005 Influence of process variables on electron beam chemical vapor deposition of platinum *J. Vac. Sci. Technol.* B **23** 2151

[6] Ding W, Dikin D A, Chen X, Piner R D, Ruoff R S, Zussman Z, Wang X and Li X 2005 Mechanics of hydrogenated amorphous carbon deposits from electron-beam-induced deposition of a paraffin precursor *J. Appl. Phys.* **98** 014905

[7] Shimizu R and Ding Z J 1992 Monte Carlo modeling of electron–solid interactions *Rep. Prog. Phys.* **55** 487

[8] Dapor M 1992 Monte Carlo simulation of backscattered electrons and energy from thick targets and surface films *Phys. Rev.* B **46** 618

[9] Ding Z J and Shimizu R 2000 Monte Carlo simulation study of reflection-electron-energy-loss-spectroscopy spectrum *Phys. Rev.* B **61** 14128

[10] Silvis-Cividjian N, Hagen C W and Kruit P 2005 Spatial resolution limits in electron-beam-induced deposition *J. Appl. Phys.* **98** 084905

[11] Liu Z Q, Mitsuishi K and Furuya K 2005 Three-dimensional nanofabrication by electron-beam-induced deposition using 200-keV electrons in scanning transmission electron microscope *Appl. Phys.* A **80** 1437

[12] Silvis-Cividjian N, Hagen C W, Leunissen L H A and Kruit P 2002 The role of secondary electrons in electron-beam-induced-deposition spatial resolution *Microelectron. Eng.* **61/62** 693

[13] Mitsuishi K, Liu Z Q, Shimojo M, Han M and Furuya K 2005 Dynamic profile calculation of deposition resolution by high-energy electrons in electron-beam-induced deposition *Ultramicroscopy* **103** 17

[14] Joy D C 1995 *Monte Carlo Modeling for Electron Microscopy and Microanalysis* (New York: Oxford University Press) p 25, 142

[15] Christophorou L G, Olthoff J K and Rao M V V S 1996 Electron interactions with CF_4 *J. Phys. Chem. Ref. Data* **25** 1341

[16] Winters H F and Inokuti M 1982 Total dissociation cross section of CF_4 and other fluoroalkanes *Phys. Rev.* A **25** 1420

[17] Allen T E, Kunz R R and Mayer T M 1988 Monte Carlo calculation of low-energy electron emission from surfaces *J. Vac. Sci. Technol.* B **6** 2057

[18] Crozier P A, Tolle J, Kouvetakis J and Ritter C 2004 Synthesis of uniform GaN quantum dot arrays via electron nanolithography *Appl. Phys. Lett.* **84** 3441

[19] Kohlmann-von Platen K T, Chlebek J, Weiss M, Reimer K, Oertel H and Brünger W H 1993 Resolution limits in electron-beam induced tungsten deposition *J. Vac. Sci. Technol.* B **11** 2219

[20] Fowlkes J D, Randolph S J and Rack P D 2005 Growth and simulation of high-aspect ratio nanopillars by primary and secondary electron-induced deposition *J. Vac. Sci. Technol.* B **23** 2825

[21] Bret T, Utke I and Hoffmann P 2005 Influence of the beam scan direction during focused electron beam induced deposition of 3D nanostructures *Microelectron. Eng.* **78/79** 307